Clay Li and Nd isotopes response to hydroclimate changes in the Changjiang (Yangtze) basin over the past 14,000 years

Chengfan Yang, Nathalie Vigier, Shouye Yang, Marie Revel, Lei Bi

Clay Li and Nd isotopes response to hydroclimate changes in the Changjiang (Yangtze) basin over the past 14,000 years

Chengfan Yang [a, b*], Nathalie Vigier [b], Shouye Yang [a], Marie Revel [c], Lei Bi [a, d]

a State Key Laboratory of Marine Geology, Tongji University, 1239 Siping Road, Shanghai 200092, P R China

b Oceanography Laboratory of Villefranche (LOV), IMEV, CNRS, Sorbonne University, 06230 Villefranche-sur-Mer, France

c Université Côte d'Azur, CNRS, Observatoire de la Côte d'Azur, IRD, Géoazur, 250 rue Albert Einstein, 06905 Sophia Antipolis, France

d Polar Research Institute of China, 451 Jinqiao Road, Shanghai 200136, P R China

* Corresponding author: Chengfan Yang (cfyang@tongji.edu.cn)

Abstract

In large river basins, the relationship between silicate weathering and climate variability on various temporal scales is still highly debated. This study presents clay Li-Nd isotopes and elemental compositions of bank sediments from the Changjiang (Yangtze) River, and of sediments from core CM97 recovered from its delta. In the modern basin, clay δ^7Li and ε_{Nd} values of bank sediments range from -4.1‰ to 0.9‰ and from -13.1 to -10.7, respectively. In core CM97, clay δ^7Li and ε_{Nd} values vary from -2.5‰ to -1.1‰ and from -12.7 to -11.9. We infer that the variations of clay Li isotope compositions are mostly indicative of weathering intensity changes in the Changjiang basin, and are little influenced by mineralogical sorting, lithology and early diagenesis. Over the last 13 kyr, three periods with distinct clay mineralogy and geochemical compositions can be identified. During the Younger Dryas, the positive excursion of clay δ^7Li (by ~1.4‰) is consistent with enhanced incongruent weathering of silicates (i.e., weakened weathering intensity) in the mid-lower Changjiang basin, likely due to climate cooling. The minor variation of clay δ^7Li (average -1.6 ± 0.2‰) at 11 – 2 ka confirms the small changes of weathering conditions, which is consistent with mild climatic variations. Over the last 2 kyr, isotopic fluctuations are best explained by sediment source changes, which might be caused by the intensification of human activities in the mid-lower basin. Overall, this study supports a rapid response of silicate weathering to hydroclimate changes on millennium timescale in large catchments. It also provides new insights on Li isotope fractionations at the continental scale during the Quaternary period.

Keywords: Li and Nd isotopes; clay; Changjiang River; Yangtze; continental weathering; paleoclimate

1. Introduction

Chemical weathering of silicates plays a key role in shaping Earth's surface landscape and modulating biogeochemical cycles (Gaillardet et al., 1999), and it is also one of the most important mechanisms for global climate stabilization (Raymo and Ruddiman, 1992; Frings, 2019). During this process, large amounts of sediments are transported by rivers into marginal seas or deep oceans, and potentially record continental weathering and hydroclimatic variations on various temporal scales. For instance, Lupker et al. (2013) interpreted the Bay of Bengal record as reflecting enhanced weathering intensity and weathering rate since ~21 ka, in response to more favorable Holocene climate than in the Last Glacial Maximum. Similar studies were also carried out worldwide, such as in the Changjiang (Yangtze) Delta and in the Nile Delta (Wang and Yang, 2013; Bi et al., 2017; Bastian et al., 2017).

The large river basins cover significant proportions of continental crust and various climatic regimes, and thus give advantages of studying weathering on a global scale (e.g., Gaillardet et al., 1999). However, the complex sediment source-to-sink processes and sedimentary recycling challenge our understanding of both the kinetic and the amplitude of continental weathering response to climatic variability. For instance, the comminution age of fine siliciclastic sediments (<50 μm) in the Changjiang basin can reach 300–400 kyrs (Li et al., 2016). Then, significant time lags may exist in sediment records between weathering proxies and climate variations in large catchments. On the other hand, several lines of evidences have suggested that the weathering-climate feedback observed in sediment records could be ascribed to

the changes of sediment sources caused by different erosional patterns within the basin or changes in the sedimentary dynamics during transport (Bi et al., 2017; Wan et al., 2017; Frings, 2019). In spite of these issues, there are examples indicating nearly synchronous co-variations between weathering and paleoclimate variability (Lupker et al., 2013; Bastian et al., 2017). In particular, during specific Quaternary hydroclimate events, negligible changes of clay sources were observed in Nile Delta (Bastian et al., 2017). Overall, the mechanisms and feedbacks linking silicate weathering to climate through time need to be further investigated at large scale.

During the last decade, Li isotopes have been considered as one of the most powerful proxies for silicate weathering investigation. Li is predominantly derived from weathering of silicate rocks, even in carbonate dominated catchments (Huh et al., 1998; Kısakűrek et al., 2005). Li cation is monovalent and not affected by redox reaction. During weathering processes, primary mineral dissolution shows no significant Li isotope fractionation, which has been verified by laboratory experiments (Pistiner and Henderson, 2003; Wimpenny et al., 2010; Verney-Carron et al., 2011) and by field studies (Ryu et al., 2015). In contrast, secondary minerals preferentially incorporate the light ^{6}Li, leaving isotopically heavy ^{7}Li in river water (Huh et al., 1998; Wang et al., 2015). Hence, Li isotope compositions (δ^{7}Li) are primarily controlled by the ratio of primary mineral dissolution to the secondary mineral formation. This ratio has been described as weathering congruency or intensity, with congruent weathering (i.e., high ratio) leading to low δ^{7}Li, close to the compositions of bedrock (e.g., Misra and Froelich, 2012; Bastian et al., 2017; Pogge

von Strandmann and Henderson, 2015; Pogge von Strandmann et al., 2017). Recently, Li isotopes were used to decipher weathering-climate relationship over the geologic past, which suggest distinct response to climate variation. The increase of δ^7Li values in the middle-upper Datangpo Formation (Guizhou province, South China) is consistent with an initiation of global cooling before the Marinoan glaciation (Wei et al., 2020). In the Nile basin, Bastian et al. (2017) observed higher clay δ^7Li values during several arid periods over the last 30 kyr. In contrast, clay δ^7Li displays low values during the last glacial period in sediments from Himalayan terraces (Dosseto et al., 2015). To date, it is still unclear how sediment δ^7Li, silicate weathering and climate are related over the geologic past.

As the largest and longest river in Asia, the Changjiang River originates from the Tibetan Plateau, and flows eastward into the East China Sea. The Changjiang Delta, as one of the major sinks of river sediments, preserves high-resolution sedimentary records for the Holocene environmental changes in this large catchment. In this study, we report clay Li and Nd isotopes and element concentrations in core CM97 recovered from the Changjiang Delta and in modern river bank sediments (Fig. 1). In combination with published paleoclimatic records in this region, we investigate how riverine clay Li isotopes may indicate changes in silicate weathering as a function of climatic variations in large river systems.

2. Regional background

The Changjiang, as one of the largest rivers in the world, originates from the

Tibetan Plateau at an elevation above 5,000 m, and drains central China with a length of ca. 6,300 km and a catchment area of 1.8×10^6 km^2 (Fig. 1A). The annual average sediment flux was 470 Mt, which represents ca. 2.5% of present-day estimate for the global sediment flux (Milliman and Farnsworth, 2011). Its drainage basin spans three-grade physiographic terraces in China, with average elevations of 3,000 – 5,000 m, 500 – 2,000 m and less than 500 m respectively (Fig. 1C). According to hydrological and geographic settings, the Changjiang drainage basin is generally divided into three sections. The upper reaches are the section from river source to City Yichang (Fig. 1B), which are mostly located at the first and second-grade physiographic terraces. Before dam constructions in 2003, the upper reaches contributed at least 70% of the annually sediment flux to the East China Sea (Yang Z et al., 2006). The mid-lower reaches are from City Yichang to the river mouth, mostly <500 m in altitude (Fig. 1B). The floodplain and alluvial plains are well developed, occupying about 44% of the total basin area. The Dongting and Poyang Lakes are two major contributors of sediments into the modern Changjiang mainstream in the middle basin (Fig. 1B).

Geologically, the Changjiang drainage basin is primarily located in the South China Block, which is composed of the Yangtze Craton and the Cathaysia Block (Fig. 1A). It is bounded by the Qinling-Dabie orogenic belt to the north and by the Songpan-Garze terrain to its northwest. The intermediate, basic (e.g., Emeishan basalt province) and ultra-basic rocks are mainly distributed in the upper basin (Fig. 1B). The Changjiang catchment is strongly affected by the humid sub-tropical Asian

monsoon climate, that is warm and humid in summer and cold but arid in winter. Generally, the upper basin is subject to the Indian Summer Monsoon (ISM), while the East Asian Summer Monsoon (EASM) dominates climatic changes in the mid-lower basin. At present, the period from May to October accounts for more than 70% of annual water discharge, with a peak mostly in July. Spatially, the annual precipitation increases eastward, from < 400 mm/yr in east Tibet, to about 1000 mm/yr at Chongqing and > 2,000 mm/yr in lower reaches. The mean annual precipitation over the whole basin is ~1,100 mm, and the water discharge into the sea is about 900 km^3/yr. Except for the cold climate (below 4°C) in the river source area, the mean annual temperature in the mid-lower basin is about 16 – 18°C.

At the last deglaciation, the sea-level in the East China Sea was about 120 m below the present-day position (Fig. 1D), and the modern river mouth was occupied by a huge incised valley at that time, with the width and depth up to 70 km and 80 m, respectively (Li et al., 2002). With the postglacial sea-level rise, the incised valley was gradually filled by the Changjiang-derived sediments. During this period, the annual sediment mass deposited in the Changjiang estuarine and coastal areas was estimated to be 137 – 224 Mt/yr (Wang et al., 2018). With the sea-level reaching its highstand at 7 – 6 ka, the annual sediment influx was about 99 – 113 Mt/yr (Fig. 1D) and the modern delta initiated. During the last 2 kyr, strong human activities caused the annual sediment flux increasing to 162 Mt/yr on average.

3. Materials and methods

3.1. Samples

Core CM97 (~70 m in depth) was drilled at the modern Changjiang River mouth (31°370’ N, 121°230’ E) in 1997. The AMS ^{14}C dating on molluscan and/or snail shells was reported by Hori et al. (2001), and then the age model was gained using linear interpolation. Core CM97 thus records the depositional history over the past ~14,000 years, and the sedimentary sequence primarily consists of fluvial and floodplain facies at the bottom (70 – 60.3 m in depth), estuarine to shallow marine facies in the middle part (60.3 – 20.1 m), and deltaic facies at the top (20.1 – 0 m). The detailed information about sedimentary facies was described in Hori et al. (2001). In this study, a total of 61 samples were selected from core CM97 for geochemical measurements. After this, in order to constrain the provenance of core sediment, 11 riverine bank samples, including 5 from the upper reaches, 3 from the Dongting and Poyang Lake in the middle basin, and 3 from the lower reaches, were taken in May and July, 2018 (Fig. 1B).

3.2. Clay fraction (<2 μm) separation and Li isotope analyses

About 1 g bulk sediment was first separated into two groups (i.e., > 63 μm sand fraction and < 63 μm fine-grained fraction) using wet sieving method. Then, the fine-grained fraction (<63 μm) was immersed into 20 ml 1N HCl for twenty minutes to remove carbonates at room temperature. This method is effective enough for carbonate removal. Carbonate is generally Li-poor (1-2 μg/g), but the use of HCl acid may remove some Li from Fe-Mn oxides/hydroxides (Bi et al., 2017). In this study,

we calculate that a maximum of ~6% of sedimentary Li is removed at this step, by comparing Li concentrations before and after HCl leaching. The residue was washed three or four times with Milli-Q water until the supernatant pH reached neutral value. Afterwards, the clay fraction was separated from the fine-grained fraction by the pipette method following the Stoke's Law at room temperature. In order to remove exchangeable Li, the clay fraction was mixed with 20 ml 1 N Ammonia Chloride (NH_4Cl) solution (Vigier et al., 2008). Finally, the clay fraction was freeze-dried after washing twice with Milli-Q water.

About 10 mg of clay samples were ground to <200 mesh in an agate mortar and then were digested first using 3:1 HF/HNO_3 solution at 70°C for several hours. Afterwards, the solution was evaporated and re-dissolved with concentrated HNO_3 several times. The sample was then re-digested with 3:1 HCl/HNO_3 solution. Finally, the solution was evaporated and re-dissolved in 4 ml 1 N HCl. At this stage, the solution was systematically centrifuged to ensure the lack of any solid residue. The Li purification was performed on a cationic resin column, following the method described in Vigier et al. (2008). All of these experiments described above were conducted at Laboratory of Oceanography of Villefranche-sur-Mer (LOV), Sorbonne University. Li isotopes measurement were performed using a MC-ICP-MS Neptune plus (Thermofisher) at the Ecole Normale Supérieur de Lyon (National Facilities). The accuracy of the isotopic measurements was monitored by analyzing Li7-N pure Li solutions and BE-N basaltic rocks. Repeated measurements yielded mean δ^7Li value of +30.3 ± 0.6‰ (2SD, n=26) and +5.2 ± 0.5‰ (2SD, n=4), respectively. In

addition, three samples were processed repeatedly using the same but independent chemical procedure, yielding values of -1.9 ± 0.4‰ (2SD, n=3), -1.5 ± 0.3‰ (2SD, n=3) and -1.3 ± 0.2‰ (2SD, n=3), respectively (Table S2). Thus, the external reproducibility for silicate materials ranges from 0.2‰ to 0.5 ‰ at the 2σ level

3.3. Al, Na and Li concentrations and Nd isotope analyses

About 50 mg powder samples were ignited in muffle furnace at 600°C in order to remove organic matter before acid digestion. Afterwards, these powder samples were dissolved with a mixture of 1:1 concentrated HNO_3 and HF in a tightly closed Teflon vessel for at least 48 h with a temperature of 190°C. After drying, samples were re-dissolved in HNO_3 to break down any fluorides. Finally, samples were re-digested in 2 ml 30% HNO_3 with a temperature of 190°C. The concentrations of Al and Na were measured respectively by Inductively Coupled Plasma-Optical Emission Spectrometers (ICP-OES, IRIS Advantage), and of Li by Inductively Coupled Plasma Mass Spectrometry (ICP-MS, Agilent 7900) at the State Key Laboratory of Marine Geology, Tongji University. The analytic precision and accuracy were monitored by rock standards of BCR-2. The results showed that the precision and accuracy of elements is generally less than 5%, while Li concentration has an accuracy of 10%.

The Nd purification was conducted with a two-step method. The Rare Earth Elements (REE) were first separated using 2.5 N HCl elution on an ion-exchange column filled with Bio-Rad AG50W-X12, 200-400 mesh resin. Then, the Nd was separated from the REE solution using 0.25 N HCl. Finally, the Nd isotope ratios

were determined using a MC-ICP-MS Neptune plus at the State Key Laboratory of Marine Geology, Tongji University. In this study, Nd isotope values are reported as ε_{Nd}, which is equal to $[(^{143}Nd/^{144}Nd)_{samples}/(^{143}Nd/^{144}Nd)_{CHUR}-1] \times 10^4$. The CHUR represents Chondritic Uniform Reservoir, with a value of 0.512638. The mean measured ε_{Nd} of BCR-2 is 0.0 ± 0.3 (2SD, n=10), well within the recommended values.

4. Results

The Li concentrations of clay fractions from CM97 sediments range from 78.6 μg/g to 99.1 μg/g, with an average of 88.0 ± 5.4 μg/g (Table 1). Their δ^7Li values vary between -2.6‰ and -1.1‰ (Table 1), systematically lower than the average of +0.6 ± 0.6‰ estimated for the upper continental crust (Sauzéat et al., 2015). As for the modern bank sediments, clay δ^7Li of upstream-derived sediments vary from -0.3‰ to 0.9‰ (Table 2). These values are comparable with those reported for sedimentary rocks in the Tibetan Plateau (Weynell et al., 2017), and are within the range for the upper continental crust (Fig. 2A). In comparison, the Li isotope compositions of clay-size sediments collected in the Dongting and Poyang basins are lighter, ranging from -4.1‰ to -2.3‰ (Fig. 2A). As already demonstrated by Wang et al. (2015), the δ^7Li values of SPM samples collected in the upper Changjiang reaches are also higher than those in Dongting and Poyang Lakes (Fig. 2A). The ε_{Nd} values of clay fractions separated from core CM97 sediments show a narrow but significant variation, ranging from -12.8 to -11.6 (Fig. 2B). This is within the range measured for modern

Changjiang river sediments (Yang et al., 2007; He et al., 2015). Clay ε_{Nd} values vary from -11.5 to -10.7 in the upper reaches, and from -15.2 to -12.4 in the Dongting and Poyang Lake regions (Table 2). Clay ε_{Nd} values in the lower reaches range from -12.2 to -11.7. The difference in clay ε_{Nd} between the upper reaches and the middle basin is larger than the analytical uncertainty (0.3, 2SD), making possible to use this proxy for assessing the sediment provenance.

5. Discussion

5.1. Clay provenance and depositional environments

The provenance of core CM97 sediments has already been estimated using clay mineral assemblages and bulk sediment Sr-Nd isotope compositions (Wang and Yang, 2013; Bi et al., 2017). These results indicated that sediments accumulated in the Changjiang Estuary typically represented an average composition of particulates from the whole Changjiang basin (mainly from the mountainous upper reaches, as well as from the middle basin). Nd isotopes are thought to be independent of Earth surface processes (e.g., chemical weathering and hydrodynamic sorting), and thus are widely used to discriminate river sediment sources (e.g., Bayon et al., 2015; Revel et al., 2015). Given that the Changjiang basin is tectonically stable since the late Pleistocene (Yang S et al., 2006), the provenance of core CM97 clay fraction can be determined by comparing their Nd isotope compositions with those of modern river sediments. The Permian basalts widely distributed in the upper Changjiang basin are characterized by relatively higher ε_{Nd} values, compared to those of granites and

Quaternary fluvial-lacustrine sediments in the mid-lower basin (Yang et al., 2007; He et al., 2015). Accordingly, the ε_{Nd} values of the Changjiang sediments decrease downstream with increasing sediment contribution from the mid-lower basin (Yang et al., 2007). As shown in Figure 3B, the content ratios of kaolinite to illite (i.e., kaolinite/illite) are also shown for comparison (Wang and Yang, 2013). At present, illite accounts for 60 – 80% of clay mineral assemblages in the upper Changjiang basin, while sediments from the Dongting and Poyang regions in the middle basin are featured by relatively higher kaolinite contents, in relation with more intensive weathering conditions therein (He et al., 2013). Thus, at a first approximation, kaolinite/illite ratios indicate a source effect (i.e., sediment from the upper basin or the middle basin). Indeed, warm and humid climate favors kaolinite formation. Considering the climatic evolution over the past 14 kyr, we therefore suggest that the kaolinite/illite ratio in core CM97 can be affected by changes of silicate weathering in the Changjiang basin as well.

As illustrated in Figure 3A, clay ε_{Nd} values show a limited variation at 13 – 2 ka and a negative shift during the last 2 kyr. It is worth noting that the negative excursions of clay ε_{Nd} at 4.3 – 4.1 ka are small but larger than analytical uncertainty, suggesting more clay contributions from the middle basin during this period. This result is consistent with the observation from kaolinite/illite ratio, which shows stable values at 11 – 2 ka but higher values at 2 – 0 ka (Fig. 3B). This consistency between clay ε_{Nd} and kaolinite/illite ratios evidence a significant change of the sediment source during the last 2 kyr, with a greater but fluctuating contribution from the middle

Changjiang basin. In contrast, at 13 – 11 ka (i.e., Younger Dryas period), kaolinite/illite ratio displays a slightly decreasing trend, while clay ε_{Nd} variation remains stable. This may feature a progressive shift of chemical weathering conditions during the Younger Dryas, which we will be investigated further using Li isotopes (section 5.3).

With the sea-level rise during the last deglaciation, the local depositional environment has greatly changed in the Changjiang Delta. The sedimentary system in the East China Sea shifted from the transgressive system tract in the last deglaciation (15.4 – 7 ka) to the highstand system tract since 7 ka (Hori et al., 2001; Li et al., 2002). Correspondingly, in the core CM97, the fluvial facies, estuarine to shallow marine facies, deltaic facies and their respective sub-facies can be subsequently observed (Fig. 1E). The changes in depositional environment may significantly affect provenance discrimination and weathering information recorded by core sediments. For instance, as shown in Figure 3C, 3D and 3E, bulk ε_{Nd} values are higher in coarser sediments at periods with higher sedimentation rates (i.e., at 13 – 11 ka and 2 – 0 ka). In contrast, clay ε_{Nd} values appear independent from the variation of mean grain size and sedimentation rate. Hence, there is an apparent inconsistence for sediment source between clay fraction and bulk sediments in core CM97. This inconsistency is best explained by a different transport and deposition between coarse-grained sediments and clays. Fine-grained clays are transported more rapidly and likely less sensitive to these physical processes. These observations strongly suggest that geochemical compositions of bulk sediments can be largely affected by depositional environment

and sea-level changes, while fine clays remain less sensitive to these aspects, as suggested by study in the Nile Delta (Bastian et al., 2017).

5.2. Grain size, lithological, estuarine and diagenetic effects on clay δ^7Li

In this study, in order to minimize grain size effect, we focused on clay fractions. Li is generally more concentrated in clay minerals, and coarse-grained quartz and feldspar are Li-poor host (Dellinger et al., 2014; Sauzéat et al., 2015). Indeed, Li and δ^7Li in riverine sediments, even in fine suspended particulate matter, can be strongly influenced by a mixing between various primary minerals and weathering products (e.g., Dellinger et al., 2014, 2017). The Changjiang basin is characterized by igneous and sedimentary rocks, while high-grade metasedimentary rocks are distributed sporadically (Yang et al., 2007). As illustrated in Figure 4A, the geochemical compositions of SPM samples and bulk sediments of core CM97 both show a binary mixing between igneous end-member and weathering products. In contrast, δ^7Li values and Li concentrations measured in clay fractions are clearly distinct from this mixing pattern (Fig. 4). This implies that elemental and isotopic variations in clay samples are not derived from mixing with igneous rocks. Compared to the bulk sediments, the clay fraction and fine-grained sediments in general (as also shown in Dellinger et al., 2017) are more likely to contain a higher proportion of contemporaneous weathering products (i.e., soil-derived clays). This observation therefore strongly supports the use of clay fraction as a tracer of continental weathering. However, the trend defined by clay fraction also demonstrates some

potential influences from recycled sedimentary rocks, i.e. recycled clays derived from sedimentary rocks (Fig. 4). In the Changjiang basin, illite is the most abundant clay minerals in upstream sediments (He et al., 2013), and is mostly eroded from recycled sedimentary rocks (Weynell et al., 2017). Kaolinite is a weathering product that is mainly produced in the middle Changjiang basins (He et al., 2013). To some extent, the influence of recycled sedimentary rocks on chemical weathering can thus be roughly estimated by kaolinite/illite ratios.

Estuarine processes may also affect the geochemical compositions of deposited particles and sediments. Due to the difference in ionic strength, pH and temperature between river and sea water, chemical compositions of riverine sediments can be modified in the estuary by adsorption-desorption, particle dissolution and/or ongoing weathering processes (Gislason et al., 2006; Jeandel and Oelkers, 2015). For Li isotopes, there is no consensus about the influence of these processes, and only few studies have been published. In Iceland, Pogge von Strandmann et al. (2008) observed an increase of SPM δ^7Li values (from ~0‰ to ~5‰) along a transect in the Borgarfjörður estuary, and related this to ongoing weathering of particles with seawater. Based on the investigation of sedimentary facies, the location of core CM97 was suggested to be inundated since ~9 – 10 ka due to sea-level rise (Hori et al., 2001; Li et al., 2002). However, clay δ^7Li values fluctuate around -1.5‰ during the middle Holocene under the maximum marine transgression (Fig. 5A), and show no positive or negative excursion in response to ongoing reaction with seawater or particle dissolution. Additionally, any adsorbed Li onto clay or Fe-Mn oxyhydroxides surface

has been removed using NH_4Cl solution (see section 3.2). Thus, estuarine processes did not visibly alter clay δ^7Li values over the studied period of time.

Early digenesis is another process that may be associated to the uptake of Li from seawater (δ^7Li = 31.2‰), with a non-negligible isotope fractionation (Misra and Froelich, 2012). Clay δ^7Li values of core CM97 should vary with the proceeding of diagenesis, as authigenic clays generated from seawater are expected to result in higher δ^7Li values relative to continental weathering products (Wei et al., 2020). However, there is no systematic increase or change of the clay δ^7Li value as a function of depth or of the sediment age (Fig. 5A). Also, in Figure 4, most clay data plot close to the shale end-member (Fig. 4). These observations therefore strongly suggest that early digenesis was not significant enough to alter the clay δ^7Li values inherited from continental process. In fact, these relatively young detrital clays contain large amounts of lithium, which may mask the signal from minor lithium addition or loss potentially associated with early diagenesis.

5.3. Assessing links between weathering and climatic variation

As illustrated in Figure 5A, core CM97 clay δ^7Li values exhibit a small but statistically significant increase of ~1.4‰ during the Younger Dryas (YD) from 13 ka to 11 ka. Then, relatively stable δ^7Li values (compared to the external reproducibility) are punctuated by excursions at three short-term periods between 11 ka and 2 ka. These excursions occurred at 4.2 – 4.1 ka, 8.6 – 8.1 ka, 10.5 – 10.1 ka, possibly corresponding to the 4.2 ka, the 8.2 ka, the 10.3 ka climate events (Wanner et al.,

2011). However, the ^{14}C ages used in this study may bear large uncertainties, and the temporal resolution is not sufficient to confirm if these fluctuations correspond to these specific climate events. Thus, the mechanism for clay δ^7Li variations on centennial timescales will not be further discussed in the following. During the last 2 kyr, larger fluctuations of clay δ^7Li (between -1.1‰ and -2.5‰) can be observed (Table 1).

5.3.1. Impact of climate cooling during the Younger Dryas

The YD event corresponds to millennium-scale climate cooling, and punctuated the termination of the last glacial period at 12.9 – 11.7 ka. During this period, the temperature in central China was estimated to be ~2 – 4°C lower, based on branched fatty alcohol ratio (BNA15) measured in Dajiuhu peatland (Fig. 5E; Huang et al., 2013). According to paleoclimatic records recovered from Tiancai lacustrine sediments (Zhang et al., 2017), the temperature decrease was also observed in the upper Changjiang basin (Fig. 5D).

As a first approximation, the positive excursion of clay δ^7Li during the YD period could be caused by a change of Li isotope fractionation factor, as it is temperature-dependent (Vigier et al., 2008). However, a temperature decrease would rather lead to a decrease in clay δ^7Li values (Vigier et al., 2008). Then, a change of sediment source can be envisioned, but this is not consistent with the minor changes of clay ε_{Nd} values during this period (Fig. 5C). We therefore propose that the variation in core CM97clay δ^7Li during the YD period is most likely indicative of changes in

silicate weathering intensity in response to climatic evolution. As Li is quantitatively incorporated into the secondary minerals, clay δ^7Li values primarily depend on the ratios of primary mineral dissolution to secondary minerals formation. Higher temperature is expected to increase the congruency of weathering, as the solubility of most primary minerals increases with temperature (Pogge von Strandmann et al., 2017). Conversely, the climate cooling during the YD period appears consistent with more incongruent weathering conditions (i.e., weakened weathering intensity), resulting in higher clay δ^7Li values. The decreasing trend of kaolinite/illite ratio during the YD period (Fig. 5B) supports this interpretation, since less kaolinite formed in the middle Changjiang basin is consistent with a cool climate.

5.3.2. Impact of Holocene monsoon variability between 11 ka and 2 ka

As mentioned above (Fig. 1A), the upper Changjiang basin is subject to the India Summer Monsoon (ISM), while the climate in the mid-lower basin is controlled by the East Asia Summer Monsoon (EASM). The variation of ISM is directly linked to solar insolation. In contrast, apart from solar insolation, ice volume in North Atlantic and the West Pacific subtropical high possibly exert additional forcing on the EASM (Dykoski et al., 2005, Rao et al., 2016). Consequently, the ISM and EASM show synchronous variations during the Holocene in the Changjiang basin (Figs. 5D and 5E).

Between 11 ka and 2 ka, clay ε_{Nd} variations are small compared to analytical uncertainty (Fig. 3A), which implies relatively stable source of core CM97 clay

fraction. The kaolinite/illite ratios and clay δ^7Li variations remain minor as well (Figs, 5A and 5B). Previous studies have indicated that the response of weathering intensity to climatic variation can be dampened in large river catchments (Li et al., 2016; Romans et al., 2016). Indeed, due to the long residence time of sediments, large river basins can buffer any trace of changes caused by climatic variations (Li et al., 2016; Romans et al., 2016). However, this view is not consistent with the significant variations of Li isotope observed during the YD period (Fig. 5A). Clays being the finest fraction in river sediments may be transported rapidly and reside over a much shorter timescale in the flood/alluvial plains, such as in the Nile Basin (Bastian et al., 2017). Thus, in the context of negligible sediment source changes, the minor changes of clay δ^7Li in core CM97 demonstrate insignificant variation of weathering intensity in the Changjiang basin at 11 – 2 ka. As illustrated in Figures 5D and 5E, climate variations in the Changjiang basin were mild during this period, which may explain this minor variation of continental weathering.

5.3.3. Impact of human activities during the last 2 kyr

During the last 2 kyr, clay ε_{Nd} and kaolinite/illite ratios both indicate additional clay contribution from the middle Changjiang basin as discussed in section 5.1. Thus, changes in clay source most likely account for the observed variation of clay δ^7Li in core CM97 (Fig. 5A). Over the last 2 kyr, a fast development of society and civilization is observed in the Changjiang basin (Wang and Yang, 2013; Bi et al., 2017). For instance, the reduction in trees and shrubs pollen, in parallel with a rise of

herbaceous pollen, suggest enhanced agricultural activities in the lower Changjiang basin since 3 ka (e.g., Yao et al., 2017). In the past 1,000 years, the lower Changjiang basin became a center of intensive rice production (Zong et al., 2012). Soil erosion can be strongly affected by human activities, especially by cultivation and deforestation (Wang et al., 2011). Accordingly, relative to the period between 11 ka and 2 ka, more kaolinite could be eroded from the middle basin and transported further to the Changjiang Estuary. Nevertheless, the analytical uncertainty of the ^{14}C dating and sampling resolution in this study do not allow us to further investigate the mechanism of how human activities altered the clay sediment production and transport. More direct evidences and high-resolution observations are further required for a better understanding of the anthropogenic perturbation on weathering and erosion processes in large catchments.

6. Implications and Conclusions

The glacial-interglacial cycle is of particularly importance to understand the weathering-climate relationships (Frings, 2019). However, hydrodynamic sorting, sediment recycling and long sediment residence time in the flood/alluvial plains make the interpretation of weathering proxies ambiguous, in particular for a large river basin. In this study, the Changjiang Delta provides high-resolution sediment archives for investigating weathering and climatic variation over the past 14, 000 years. Our results indicate that climate remains a major external force for silicate weathering at the continental scale. They also underline the importance to establish changes in the

444 sediment source in response to hydroclimate variations.

445 We observe that clay Li isotope compositions faithfully record the YD event,
446 while source tracers (e.g., Nd isotopes) remain constant. This strongly suggests a fast
447 response of chemical weathering to a strong climate event in the Changjiang basin.
448 The weathering signals registered by the clay fractions are less altered during
449 sediment "source-to-sink" processes because of their relatively rapid transport by
450 waters and negligible mineral sorting effect. Possibly, the comminution age calculated
451 by Li et al. (2016) for fine-grained sediments (<50 μm) in the Changjiang basin
452 concern mostly the coarser minerals (>5 – 10 um).

453 Another interesting feature is that clay δ^7Li and ε_{Nd} values fluctuate
454 significantly during the last 2 kyr, suggesting a more intensive human-induced soil
455 erosion. The minor δ^7Li and ε_{Nd} variations at 11 – 2 ka are likely caused by small
456 changes of weathering conditions, in agreement with mild climatic variations during
457 the Holocene in the Changjiang basin. Overall, the clay δ^7Li records suggest the
458 complex response of silicate weathering and clay formation in large catchments on
459 various temporal scales.

460

461 **Acknowledgements**

462 This work was funded by National Natural Science Foundation of China (Grant
463 No. 41730531, 41991324) and the ANR INTOCC project (ANR-15-CE31-0013), and
464 Shanghai Belt and Road Joint Laboratory of Sunda Shelf Drilling (No. 18230750600).
465 Chengfan Yang was supported by China Scholarship Council (CSC NO.

201706260031) for two years PhD study at the Laboratory of Oceanography of Villefranche-sur-Mer in France (LOV). We thank three anonymous reviewers for their constructive comments that contribute to greatly improve the paper quality. We thank Yalong Li for assistance with ICP-OES analyses, Chao Li, Xiangtong Huang and Ergang Lian for their help in the field work. Many thanks to the CHOC (Chemistry-Ocean-Climate) team at the LOV for their help with sample pre-treatment.

References

Bastian, L., Revel, M., Bayon, G., Dufour, A., & Vigier, N. (2017). Abrupt response of chemical weathering to Late Quaternary hydroclimate changes in northeast Africa. Scientific reports, 7, 44231.

Bayon, G., Toucanne, S., Skonieczny, C., Andre, L., Bermell, S., Cheron, S., Dennielou, B., Etoubleau, J., Freslon, N., Gauchery, T., Germain, Y., Jorry, S. J., Ménot, G., Monin, L., Ponzevera, E., Rouget, M. L., Tachikawa, K., & Barrat, J. (2015). Rare earth elements and neodymium isotopes in world river sediments revisited. Geochimica et Cosmochimica Acta, 17-38.

Bi, L., Yang, S., Zhao, Y., Wang, Z., Dou, Y., Li, C., & Zheng, H. (2017). Provenance study of the Holocene sediments in the Changjiang (Yangtze River) estuary and inner shelf of the East China sea. Quaternary International, 441, 147-161.

Dellinger, M., Gaillardet, J., Bouchez, J., Calmels, D., Galy, V., Hilton, R. G., Louvat, P., & France-Lanord, C. (2014). Lithium isotopes in large rivers reveal the cannibalistic nature of modern continental weathering and erosion. Earth and Planetary Science Letters, 401, 359-372.

Dellinger, M., Bouchez, J., Gaillardet, J., Faure, L., & Moureau, J. (2017). Tracing weathering regimes using the lithium isotope composition of detrital sediments. Geology, 45(5), 411-414.

Dosseto, A., Vigier, N., Joannes-Boyau, R. J., Moffat, I., Singh, T., & Srivastava, P. (2015). Rapid response of silicate weathering rates to climate change in the Himalaya. Geochemical Perspectives Lettes, 1(1), 10-19.

Dykoski, C. A., Edwards, R. L., Cheng, H., Yuan, D., Cai, Y., Zhang, M., Lin, Y., Qing, J., An, Z., & Revenaugh, J. (2005). A high-resolution, absolute-dated Holocene and deglacial Asian monsoon record from Dongge Cave, China. Earth and Planetary Science Letters, 233(1-2), 71-86.

Frings, P. J. (2019). Palaeoweathering: How Do Weathering Rates Vary with Climate? Elements, 15(4), 259-265.

Gaillardet, J., Dupré, B., Louvat, P., & Allegre, C. J. (1999). Global silicate weathering and CO2 consumption rates deduced from the chemistry of large rivers. Chemical geology, 159(1-4), 3-30.

Gislason, S. R., Oelkers, E. H., & Snorrason, A. (2006). Role of river-suspended material in the global carbon cycle. Geology, 34(1), 49-52.

He, M., Zheng, H., Huang, X., Jia, J., & Li, L. (2013). Yangtze River sediments from source to sink traced with clay mineralogy. Journal of Asian Earth Sciences, 69, 60-69.

He, M., Zheng, H., Clift, P. D., Tada, R., Wu, W., & Luo, C. (2015). Geochemistry of fine-grained sediments in the Yangtze River and the implications for provenance and chemical weathering in East Asia. Progress in Earth and Planetary Science, 2(1), 32.

Hori, K., Saito, Y., Zhao, Q., Cheng, X., Wang, P., Sato, Y., & Li, C. (2001). Sedimentary facies and Holocene progradation rates of the Changjiang (Yangtze) delta, China. Geomorphology, 41(2-3), 233-248.

Huang, X., Meyers, P. A., Jia, C., Zheng, M., Xue, J., Wang, X., & Xie, S. (2013).

517 Paleotemperature variability in central China during the last 13 ka recorded by a
518 novel microbial lipid proxy in the Dajiuhu peat deposit. The Holocene, 23(8),
519 1123-1129.
520 Huh, Y., Chan, L. H., Zhang, L., & Edmond, J. M. (1998). Lithium and its isotopes in
521 major world rivers: implications for weathering and the oceanic budget.
522 Geochimica et Cosmochimica Acta, 62(12), 2039-2051.
523 Jeandel, C., & Oelkers, E. H. (2015). The influence of terrigenous particulate material
524 dissolution on ocean chemistry and global element cycles. Chemical Geology,
525 50-66.
526 Kısakűrek, B., James, R. H., & Harris, N. B. (2005). Li and δ7Li in Himalayan rivers:
527 proxies for silicate weathering? Earth and Planetary Science Letters, 237(3-4),
528 387-401.
529 Li, C., Wang, P., Sun, H., Zhang, J., Fan, D., & Deng, B. (2002). Late Quaternary
530 incised-valley fill of the Yangtze delta (China): its stratigraphic framework and
531 evolution. Sedimentary Geology, 152(1), 133-158.
532 Li, C., Yang, S., Zhao, J. X., Dosseto, A., Bi, L., & Clark, T. R. (2016). The time scale
533 of river sediment source-to-sink processes in East Asia. Chemical Geology, 446,
534 138-146.
535 Lupker, M., Francelanord, C., Galy, V., Lave, J., & Kudrass, H. R. (2013). Increasing
536 chemical weathering in the Himalayan system since the Last Glacial Maximum.
537 Earth and Planetary Science Letters, 243-252.
538 Milliman, J. D., & Farnsworth, K. L. (2011). River discharge to the coastal ocean: a

global synthesis. Cambridge: Cambridge University Press

Misra, S., & Froelich, P. N. (2012). Lithium Isotope History of Cenozoic Seawater: Changes in Silicate Weathering and Reverse Weathering. Science, 335(6070), 818-823.

Pistiner, J. S., & Henderson, G. M. (2003). Lithium-isotope fractionation during continental weathering processes. Earth and Planetary Science Letters, 214(1-2), 327-339.

Pogge von Strandmann, P. A. E., James, R. H., van Calsteren, P., Gíslason, S. R., & Burton, K. W. (2008). Lithium, magnesium and uranium isotope behaviour in the estuarine environment of basaltic islands. Earth and Planetary Science Letters, 274(3-4): 462-471

Pogge von Strandmann, P. A. E., & Henderson, G. M. (2015). The Li isotope response to mountain uplift. Geology, 43(1): 67–70.

Pogge von Strandmann, P. A. E., Vaks, A., Bar-Matthews, M., Ayalon, A., Jacob, E., & Henderson, G. M. (2017). Lithium isotopes in speleothems: Temperature-controlled variation in silicate weathering during glacial cycles. Earth and Planetary Science Letters, 469: 64-74.

Rao, Z., Li, Y., Zhang, J., Jia, G., & Chen, F. (2016). Investigating the long-term palaeoclimatic controls on the δD and $\delta^{18}O$ of precipitation during the Holocene in the Indian and East Asian monsoonal regions. Earth-science reviews, 159, 292-305.

Raymo, M. E., & Ruddiman, W. F. (1992). Tectonic forcing of late Cenozoic climate.

561 Nature, 359(6391), 117.
562 Revel, M., Ducassou, E., Skonieczny, C., Colin, C., Bastian, L., Bosch, D., Migeon,
563 S., & Mascle, J. (2015). 20,000 years of Nile River dynamics and environmental
564 changes in the Nile catchment area as inferred from Nile upper continental slope
565 sediments. Quaternary Science Reviews, 130, 200-221.
566 Romans, B. W., Castelltort, S., Covault, J. A., Fildani, A., & Walsh, J. P. (2016).
567 Environmental Signal Propagation In Sedimentary Systems Across Timescales.
568 Earth-Science Reviews, 7-29.
569 Ryu, J. S., Vigier, N., Lee, S. W., Lee, K. S., & Chadwick, O. A. (2014). Variation of
570 lithium isotope geochemistry during basalt weathering and secondary mineral
571 transformations in Hawaii. Geochimica et Cosmochimica Acta, 145, 103-115.
572 Sauzéat, L., Rudnick, R. L., Chauvel, C., Garçon, M., & Tang, M. (2015). New
573 perspectives on the Li isotopic composition of the upper continental crust and its
574 weathering signature. Earth and Planetary Science Letters, 428, 181-192.
575 Teng, F. Z., McDonough, W. F., Rudnick, R. L., Dalpé, C., Tomascak, P. B., Chappell,
576 B. W., & Gao, S. (2004). Lithium isotopic composition and concentration of the
577 upper continental crust. Geochimica et Cosmochimica Acta, 68(20), 4167-4178.
578 Verney-Carron, A., Vigier, N., & Millot, R. (2011). Experimental determination of the
579 role of diffusion on Li isotope fractionation during basaltic glass weathering.
580 Geochimica et Cosmochimica Acta, 75(12), 3452-3468.
581 Vigier, N., Decarreau, A., Millot, R., Carignan, J., Petit, S., & France-Lanord, C.
582 (2008). Quantifying Li isotope fractionation during smectite formation and

583 implications for the Li cycle. Geochimica et Cosmochimica Acta, 72(3),
584 780-792.
585 Wan, S., Clift, P. D., Zhao, D., Hovius, N., Munhoven, G., France-lanord, C., Wang,
586 Y., Xiong, Z, Huang, J., Yu, Z., Zhang, J., Ma, W., Zhang, G., Li, A., Li, T.
587 (2017). Enhanced silicate weathering of tropical shelf sediments exposed during
588 glacial lowstands: a sink for atmospheric CO2. Geochimica et Cosmochimica
589 Acta, 123-144.
590 Wanner, H., Solomina, O. N., Grosjean, M., Ritz, S. P., & Jetel, M. (2011). Structure
591 and origin of Holocene cold events. Quaternary Science Reviews, 30(21),
592 3109-3123.
593 Wang, Q. L., Chetelat, B., Zhao, Z. Q., Ding, H., Li, S. L., Wang, B. L., Li, J., & Liu,
594 X. L. (2015). Behavior of lithium isotopes in the Changjiang River system:
595 Sources effects and response to weathering and erosion. Geochimica et
596 Cosmochimica Acta, 151, 117-132.
597 Wang, Q., & Yang, S. (2013). Clay mineralogy indicates the Holocene monsoon
598 climate in the Changjiang (Yangtze River) Catchment, China. Applied Clay
599 Science, 74, 28-36.
600 Wang, Z., Li, M., Zhang, R., Zhuang, C., Liu, Y., Saito, Y., Xie, J., & Zhao, B. (2011).
601 Impacts of human activity on the late-Holocene development of the subaqueous
602 Yangtze delta, China, as shown by magnetic properties and sediment
603 accumulation rates. The Holocene, 21(3), 393-407.
604 Wang, Z., Saito, Y., Zhan, Q., Nian, X., Pan, D., Wang, L., Chen, T., Xie, J., Li, X., &

605 Jiang, X. (2018). Three-dimensional evolution of the Yangtze River mouth,
606 China during the Holocene: Impacts of sea level, climate and human activity.
607 Earth-Science Reviews, 185, 938-955.
608 Wei, G., Wei, W., Wang, D., Li, T., Yang, X., Shields, G., Zhang, F., Li, G., Chen, T.,
609 Yang, T., & Ling, H. (2020). Enhanced chemical weathering triggered an
610 expansion of euxinic seawater in the aftermath of the Sturtian glaciation. Earth
611 and Planetary Science Letters, 116244.
612 Weynell, M., Wiechert, U., & Schuessler, J. A. (2017). Lithium isotopes and
613 implications on chemical weathering in the catchment of Lake Donggi Cona,
614 northeastern Tibetan Plateau. Geochimica et Cosmochimica Acta, 213, 155-177.
615 Wimpenny, J., Gíslason, S. R., James, R. H., Gannoun, A., Von Strandmann, P. A. P.,
616 & Burton, K. W. (2010). The behaviour of Li and Mg isotopes during primary
617 phase dissolution and secondary mineral formation in basalt. Geochimica et
618 Cosmochimica Acta, 74(18), 5259-5279.
619 Yang, S. Y., Li, C. X., & Yokoyama, K. (2006). Elemental compositions and monazite
620 age patterns of core sediments in the Changjiang delta: Implications for sediment
621 provenance and development history of the Changjiang river. Earth and
622 Planetary Science Letters, 245, 762-776.
623 Yang, S. Y., Jiang, S., Ling, H., Xia, X., Sun, M., & Wang, D. (2007). Sr-Nd isotopic
624 compositions of the Changjiang sediments: Implications for tracing sediment
625 sources. Science in China Series D: Earth Sciences, 50(10), 1556-1565.
626 Yang, Z., H. J. Wang, Y. Saito, J. D. Milliman, K. Xu, S. Qiao, G. Shi (2006), Dam

627 impacts on the Changjiang (Yangtze) River sediment discharge to the sea: The
628 past 55 years and after the Three Gorges Dam. Water Resour. Res., 42(4).
629 Yao, F., Ma, C., Zhu, C., Li, J., Chen, G., Tang, L., Huang, M., Jia, T., & Xu, J. (2017).
630 Holocene climate change in the western part of Taihu Lake region, East China.
631 Palaeogeography, Palaeoclimatology, Palaeoecology, 485, 963-973.
632 Zhang, E., Chang, J., Cao, Y., Sun, W., Shulmeister, J., Tang, H., Langdon, P., Yang,
633 X., & Shen, J. (2017). Holocene high-resolution quantitative summer
634 temperature reconstruction based on subfossil chironomids from the southeast
635 margin of the Qinghai-Tibetan Plateau. Quaternary Science Reviews, 165, 1-12.
636 Zong, Y., Wang, Z., Innes, J. B., & Chen, Z. (2012). Holocene environmental change
637 and Neolithic rice agriculture in the lower Yangtze region of China: A review.
638 The Holocene, 22(6), 623-635.
639

Table 1 Concentrations of Al, Na and Li and Li-Nd isotope compositions of core CM97 clay fraction

Sample ID	Age	Al	Na	Li	clay δ^7Li	clay ε_{Nd}
	cal. yr BP	wt%	wt%	µg/g	‰	
CM2.4	176	6.3	0.2	83.2	-2.5	-12.1
CM4	293	9.8	0.2	92.8	-1.3	-12.2
CM6.05	444	9.4	0.4	79.7	-1.4	-12.6
CM8.3	623	8.2	0.4	83.3	-1.7	-12.3
CM10.5	770	9.8	0.3	78.8	-1.3	-12.7
CM12.6	924	11.7	0.5	81.5	-1.6	
CM14	1027	8.1	0.4	79.5	-1.6	-12.6
CM16.3	1210	8.2	0.4	80.7	-1.9	-12.2
CM17.5	1283	11.4	0.2	86.3	-1.3	-12.8
CM18.5	1356	11.9	0.3	90.1	-1.5	
CM19.6	1437	9.2	0.3	86.4	-1.1	-12.3
CM20.7	1518	10.7	0.3	92.8	-1.2	-12.1
CM20.88	1762	10.0	0.3	88.0	-1.4	-11.9
CM20.94	1859	11.0	0.3	92.5	-1.4	-11.9
CM21.13	2165	8.4	0.2	81.7	-1.3	-11.8
CM21.23	2326	10.6	0.3	92.0	-1.6	-11.8
CM21.4	2600	10.8	0.2	90.2	-1.4	-11.7
CM21.68	3051	9.9	0.3	87.8	-1.3	-11.9
CM21.9	3406	9.4	0.3	88.8	-1.2	-12.1
CM22.07	3680	10.2	0.3	92.4		-11.8
CM22.15	3809	9.4	0.3	90.9	-1.6	-11.9
CM22.33	4099	8.2	0.3	80.3	-1.6	-11.6
CM22.37	4164	8.4	0.3	86.5	-1.1	-11.9
CM22.4	4212	9.9	0.3	94.4	-1.9	-12.3
CM22.49	4357	9.6	0.3	90.7	-1.6	-11.7
CM22.66	4621	10.3	0.3	94.6		-11.6
CM23	4816	8.5	0.3	91.2	-1.4	-12.0
CM23.7	5219	12.5	0.3	90.5	-1.4	-12.0
CM24.6	5838	8.4	0.3	95.6	-1.5	-12.1
CM24.95	6256	11.7	0.3	87.8	-1.5	-12.2
CM25.3	6689	10.5	0.3	95.6	-1.7	-11.9
CM25.5	6888	7.1	0.4	93.4	-1.4	-12.1
CM26.1	7211	9.0	0.3	97.8	-1.5	-12.1
CM26.7	7535	10.9	0.3	92.6	-1.5	-12.2
CM27.2	7805	9.5	0.2	86.4	-1.4	-12.0
CM27.54	8042	11.6	0.2	85.3	-1.5	-11.7
CM27.65	8132	8.9	0.2	80.6	-1.9	-12.0
CM27.78	8237	9.1	0.2	86.6	-1.1	-11.8
CM27.9	8335	8.3	0.3	82.6	-1.3	-12.1
CM28.3	8660	9.2	0.3	84.6	-2.0	-11.7

CM28.6	8903	10.0	0.3	92.9	-1.7	-12.2
CM29.4	9283	8.4	0.2	85.9	-1.7	-11.9
CM30.6	9466	9.3	0.2	93.5	-1.8	-12.0
CM32.3	9725	10.6	0.2	84.4	-1.6	-11.9
CM33.4	9893	10.3	0.3	94.4	-1.8	-12.0
CM35	10137	12.0	0.3	89.3	-2.2	-12.0
CM35.5	10213	9.0	0.3	78.6	-1.6	-11.9
CM36.3	10335	11.7	0.3	87.7	-1.1	-11.8
CM36.85	10419	8.7	0.3	80.9	-1.7	-12.1
CM37.5	10518	10.3	0.3	83.0	-1.9	-11.7
CM40.2	10930	9.1	0.4	84.2	-1.6	-11.9
CM42.6	11168	7.9	0.3	87.4	-1.8	-12.0
CM45.2	11426	9.0	0.3	82.9	-1.3	-12.0
CM48.3	11734	9.9	0.3	94.1	-1.2	-12.2
CM50.8	11982	8.9	0.2	96.5	-1.2	-12.0
CM53.7	12270	9.1	0.3	85.3	-1.7	-12.1
CM57.2	12617	9.3	0.3	88.1	-1.7	-12.0
CM59.3	12825	10.2	0.3	94.5	-1.9	-12.2
CM61.45	13039	12.5	0.4	91.7	-2.6	
CM64.1	13302	11.5	0.3	99.1	-2.2	
CM69.5	13838	11.6	0.5	79.9	-1.5	

640

Table 2 Li-Nd isotope compositions of clay fraction in bank sediments collected from the modern Changjiang catchment

Sample ID	Location	Longitude °E	Latitude °N	clay δ^7Li ‰	clay ε_{Nd}
CQ		106.5196	29.4228	0.3	-11.5
HJ		105.8258	28.8248	0.9	-11.3
LZ	Upper reaches	105.3709	28.8546	-0.3	-10.9
WZ		108.4267	30.7615	0.5	-11.5
YZ18YC		111.2742	30.7047	0.5	-10.7
YJCD18		111.5201	28.9361	-2.3	-13.1
YTXJ18	Middle basin	116.8014	28.4763	-3.9	-12.3
NCGJ		116.0165	28.8342	-4.1	-12.4
YZ18AQ		116.9567	30.4478	-1.1	-12.2
YZ18-ZJ	Lower reaches	119.3108	32.2011	-1.4	-11.7
YZ18NT		120.5689	32.0458	-1.4	-11.8

641

Figure captions

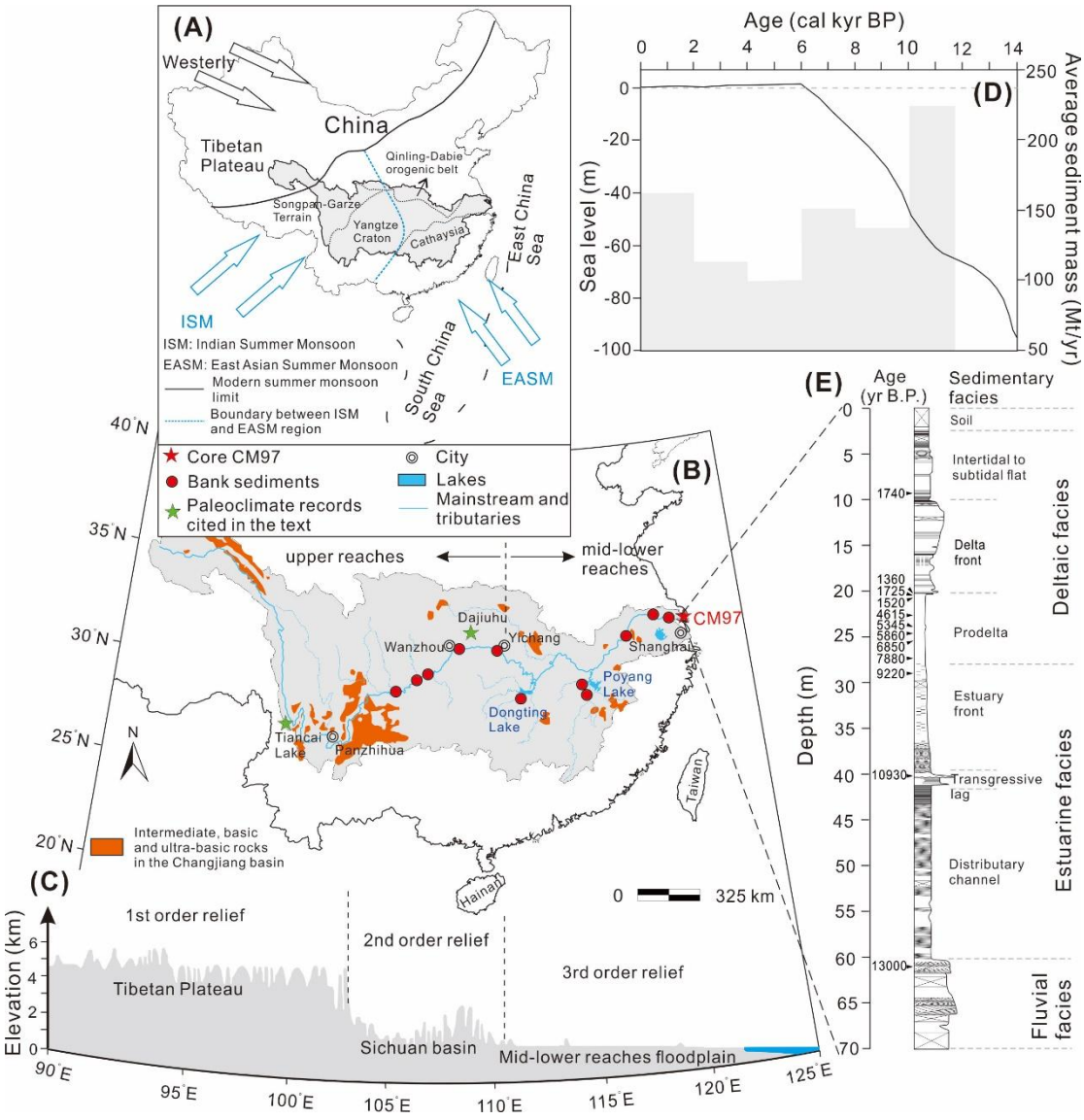

Fig. 1. Schematic map showing (A) Asian monsoon regimes, and major tectonic blocks, (B) sampling sites, drainage basin and (C) topography in the Changjiang basin. (D) The sea level changes since 14 ka in the East China Sea (Hori et al., 2001) and annual sediment mass deposited in the Changjiang estuarine and coastal areas (grey bars, Wang et al., 2018). (E) Downcore variation of sedimentary facies and depositional ages of CM97. The detailed description about sedimentary facies can refer to Hori et al. (2001).

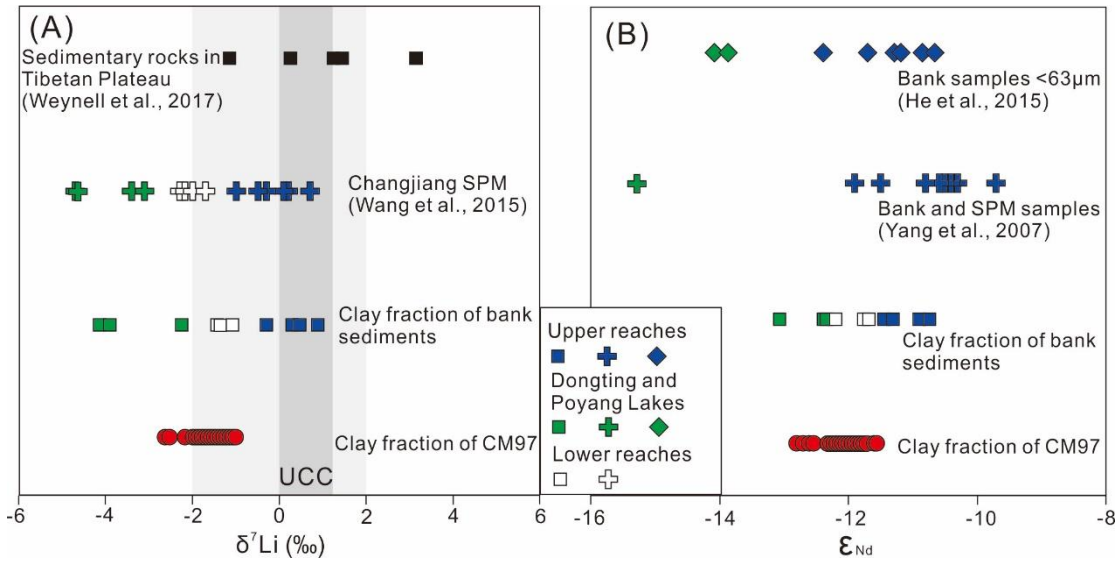

Fig. 2. (A) Li and (B) Nd isotope compositions of the sediments from the modern Changjiang River and from core CM97. δ^7Li values of suspended particulate matter (SPM) are from Wang et al. (2015). The δ^7Li values of sedimentary rocks (i.e. mudstone, sandstone and shale) collected from northeastern Tibetan Plateau are from Weynell et al. (2017). The light and dark grey bars reflect the average δ^7Li values for the upper continental crust (UCC) published by Teng et al. (2004) and Sauzéat et al. (2015), respectively. The Nd isotope compositions of SPM and bank samples are from Yang et al. (2007) and He et al. (2015). The error bar is smaller than symbol size.

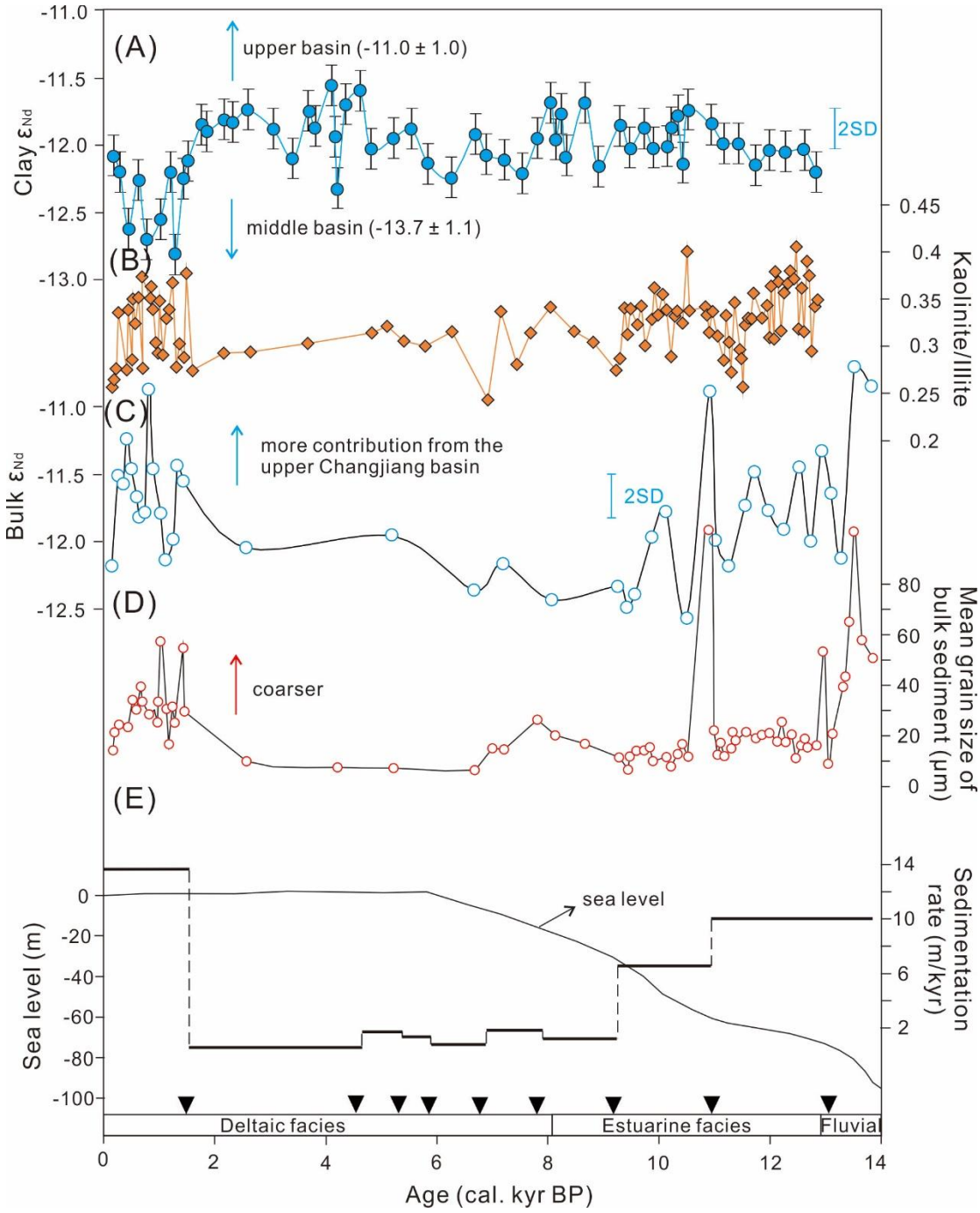

Fig. 3. (A) Clay ε_{Nd}, (B) content ratios of kaolinite to illite, (C) ε_{Nd} values in bulk sediments, (D) mean grain size of bulk sediment, and (E) mean sedimentation rate for the core CM97. The error bar for clay Nd isotope is 0.3 (2SD). The postglacial sea-level changes in the East China Sea are also shown. Sea-level changes and mean grain size are from Hori et al. (2001) and Bi et al. (2017). Kaolinite and illite contents are from Wang and Yang (2013). Bulk Nd isotope compositions are from Bi et al.

(2017). The inverted triangles represent sampling positions of molluscan shells which were used for ^{14}C dating (Hori et al., 2001). The end-member ε_{Nd} values of the upper Changjiang basin, the Dongting and Poyang Lakes are estimated by averaging data analyzed in this study and those published by Yang et al. (2007) and He et al. (2015).

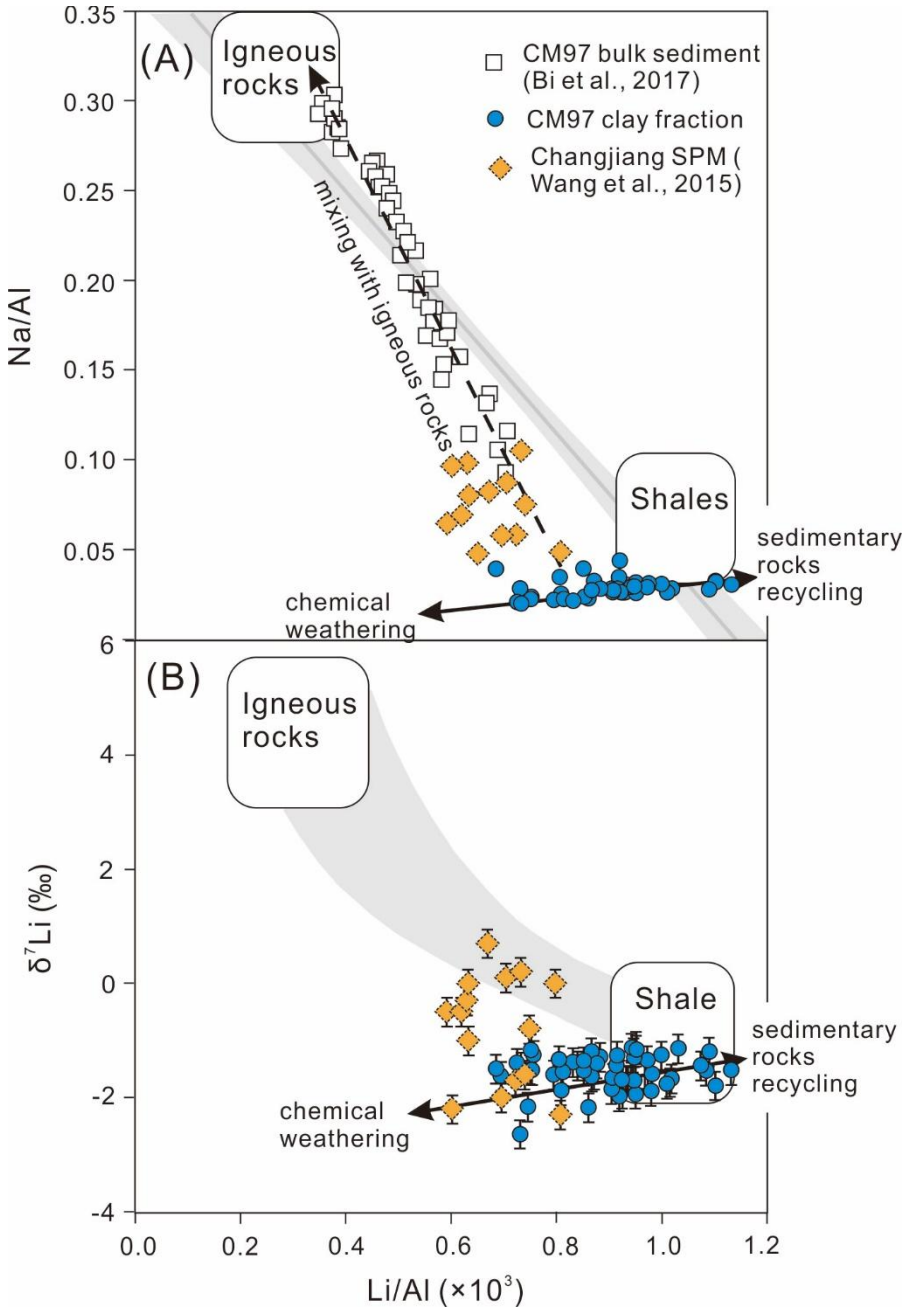

Fig. 4. (A) Na/Al ratios and (B) δ^7Li values as a function of Li/Al ($\times10^3$). The

elemental concentrations of CM97 bulk sediments and suspended particulate matter (SPM) in the Changjiang basin are cited from Bi et al. (2017) and Wang et al. (2015). The end-members of igneous rocks and shales, and the mixing line with 95% confidence interval (grey) are cited from Dellinger et al. (2014). The error bar for clay δ^7Li is 0.5‰ (2SD).

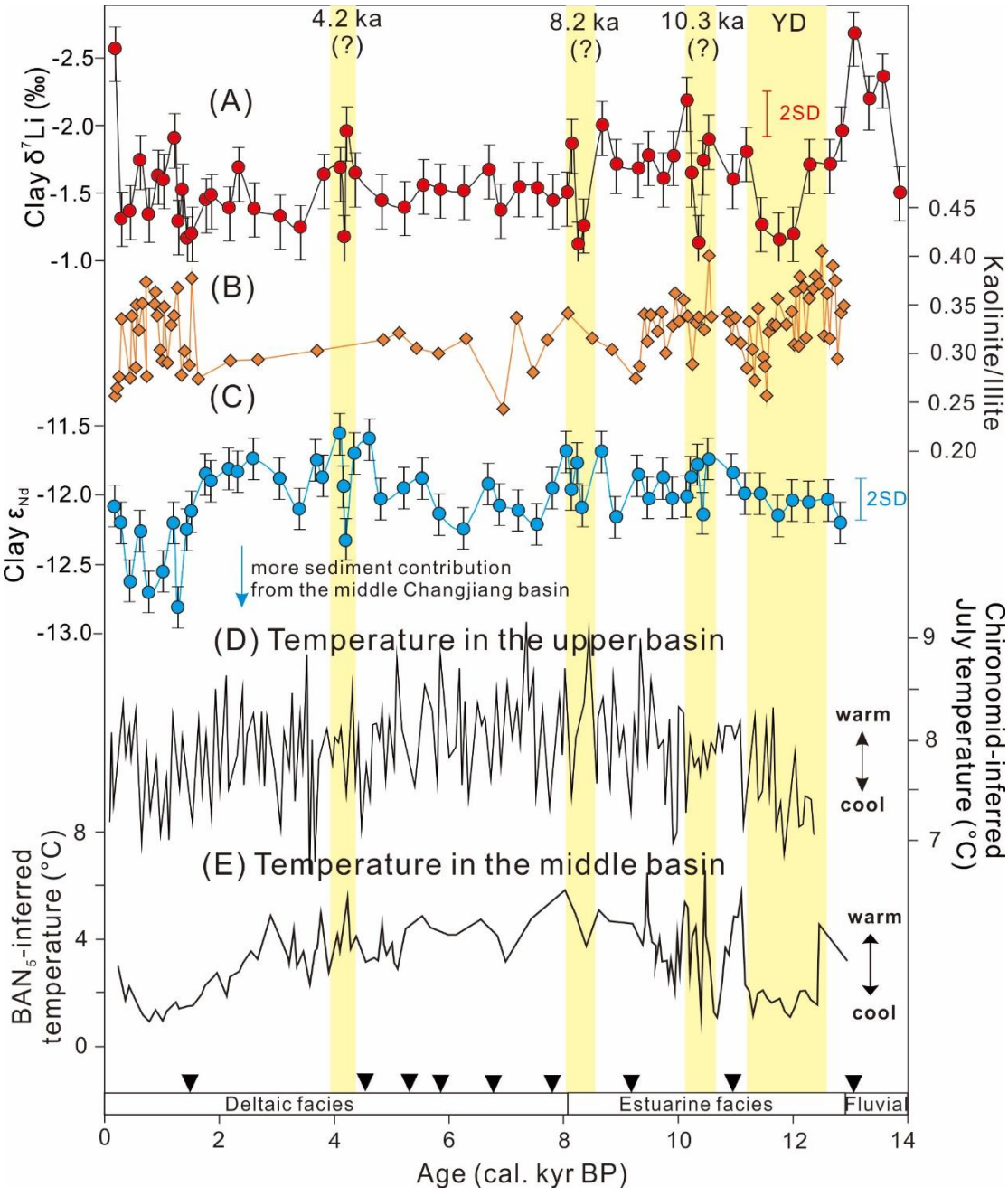

683 **Fig. 5.** Comparison of (A and C) clay Li-Nd isotopes and (B) kaolinite/illite ratios of
684 CM97 with the temperature and rainfall records in the Changjiang basin. (D)
685 Chironomid-inferred mean July temperature in Tiancai Lake, southeastern margin of
686 the Tibetan Plateau (Zhang et al., 2017). (E) Temperature reconstructed by branched
687 fatty alcohol ratio (BNA_{15}) in Dajiuhu peatland (Huang et al., 2013). The error bar for
688 clay δ^7Li is 0.5‰ (2SD).